Master-slave synchronization of hyperchaotic systems through a linear dynamic coupling

Arturo Buscarino, Luigi Fortuna, and Luca Patanè [*]
DIEEI, University of Catania, Viale A. Doria 6 Catania, 95125 Italy

(Received 26 June 2019; published 23 September 2019)

The development of synchronization strategies for dynamical systems is an important research activity that can be applied in several different fields from locomotion control of multilimbed structures to secure communication. In the presence of chaotic systems, synchronization is more difficult to accomplish and there are different techniques that can be adopted. In this paper we considered a master-slave topology where the coupling mechanism is realized through a second-order linear dynamical system. This control scheme, recently applied to chaotic systems, is here analyzed in the presence of hyperchaotic dynamics that represent a more challenging scenario. The possibility to reach a complete synchronization and the range of allowable coupling strength is investigated comparing the effects of the dynamical coupling with a standard configuration characterized by a static gain. This methodology is also applied to weighted networks to reach synchronization regimes otherwise not obtainable with a static coupling.

DOI: 10.1103/PhysRevE.100.032215

I. INTRODUCTION

Synchronization is an interesting phenomenon that emerges in coupled dynamical systems. The different time evolution of the state variables of even identical systems, due to the presence of diversities in the initial conditions, can be handled by exchanging information, typically related to an error signal, between two or more systems that can adjust their dynamics reaching a synchronous behavior [1]. Nowadays, in the research field related to nonlinear systems, there are several studies on this topic because there are multiple interesting applications ranging from physics to communication technology and control of robotic structures that can benefit from adopting reliable synchronization techniques [2–4]. Synchronization techniques are of particular importance when applied to complex nonlinear systems characterized by either a chaotic or hyperchaotic regime [5]. The high sensitivity to the initial conditions can produce completely different time evolutions in identical systems with slightly different starting values. This is an important aspect to be considered, which can be studied in simulation and then exploited in the physical realization (e.g., an electronic circuit) of the dynamical equations modeling the system [6]. Depending on the coupling strategies and on the coupling strength [7–9], it is possible to obtain different types of global synchronization, from phase to complete synchronization [1]. In some cases [10], it is even impossible to achieve the system synchronization. Coupling strategies include master-slave configuration [11], diffusive coupling [12], and system decomposition [13], all of them leading to a regime of global and complete synchronization, i.e., all systems behave following the same chaotic trajectory. More recently, different ranges of synchronization including the coexistence of different regimes, either synchronized or incoherent, have been introduced in the literature, such as chimera states [14,15] and remote synchronization [16]. These regimes are often linked to the existence of symmetries in the coupling structure and on weighted, time-varying, or weak coupling [17–19].

To evaluate the presence of a synchronization regime between the coupled systems, the master stability function (MSF) approach was introduced by Pecora and Carroll [20]. The propensity of a given dynamical system and the range of suitable coupling gain are evaluated by calculating the largest Lyapunov exponent transverse to the synchronization manifold. Adopting this technique, which is independent of the number of connected nodes and the coupling pattern, has demonstrated that hyperchaotic systems, characterized by multiple positive Lyapunov exponents, are in most cases difficult to synchronize [21]. An interesting work was proposed on the synchronization of two hyperchaotic Chen systems [22] where the error signal acquired from a single state variable is not sufficient to reach a complete synchronization. The problem was solved combining the error information coming from the multiple state variables of the coupled systems.

Among the different connection topologies, we considered a standard master-slave configuration [11] where one or more state variable error signals, calculated comparing master and slave dynamics, are used to drive the slave system through a coupling matrix modulated by a coupling strength. The master-slave approach is useful to reach synchronization in most of the cases but the range of suitable values for the coupling strength could be limited to a restricted region. To further extend the application of this synchronization scheme, the possibility to introduce a simple dynamic coupling is here investigated. We started from a recent work developed by Pena Ramirez and co-workers [23] where a second-order mass-spring-damper system was used to mediate the error signals generated to synchronize the slave system. This approach was applied to enhance the synchronization properties in oscillators and chaotic systems. We are now investigating the application of this strategy to nonlinear hyperchaotic

[*]Corresponding author: lpatane@dieei.unict.it

dynamics, which introduces a further complexity to the problem when treated with analytical tools.

Among the multitude of hyperchaotic systems designed in the last years [24], we selected two well-known systems: the hyperchaotic Chua and Saito circuits. Each system was analyzed using a simplified linear approximation to locally verify the stability of the synchronization manifold treating the nonlinear elements as a perturbation for the system [25]. The obtained results were compared with a nonlinear analysis performed through the MSF to better understand the useful indications that can be obtained and the limits of the linear analysis. Furthermore, a simple strategy to select the parameters of the dynamical coupling system is provided. The proposed method exploits information obtained from the classical coupling strategy with a static gain improving the allowable range, eliminating the upper-bound limit for the coupling strength.

The advantages introduced by the dynamic coupling were further underlined showing an application of the proposed methodology to a weighted network of hyperchaotic systems. We analyzed a network with an open chain topology characterized by three nodes and weighted directed connections. Here, the advantage characterized by the wider region of admissible coupling gains, introduced by the dynamic coupling, represents the key element to obtain the network synchronization in a case where the static coupling scheme fails in finding a suitable solution.

The paper is organized as follows: Section II describes the adopted synchronization strategy, in Sec. III the control scheme was applied to the selected hyperchaotic systems, Sec. IV proposes a discussion on the parameter selection, Sec. V presents an application to weighted networks, and finally Sec. VI draws the conclusions.

II. SYNCHRONIZATION STRATEGY

The coupling scheme considered for the synchronization of a pair of hyperchaotic systems is here discussed. The idea is based on a recent work where the synchronization of harmonic oscillators and chaotic systems is presented [23]. In our work we extended the methodology considering two identical hyperchaotic systems, connected in a master-slave configuration, where the error signal is filtered by a linear system. The role of the dynamic coupling system is schematically represented in Fig. 1 where a standard coupling mechanism, based on the state-variables feedback error modulated by a coupling gain is enhanced through the inclusion of a linear dynamical system.

Following the strategy introduced in [23], the dynamical system, representing the coupling mechanism, is modeled through a second-order linear system designed as a simple mass-spring-dumper mechanism.

The dynamic evolution of the state variables of the considered master-slave system, with the dynamic coupling, can be modeled through differential equations:

$$\begin{aligned} \dot{\mathbf{x}}_M &= \mathbf{F}(\mathbf{x}_M), \\ \dot{\mathbf{x}}_S &= \mathbf{F}(\mathbf{x}_S) - \mathbf{Ch}, \\ \dot{\mathbf{h}} &= \mathbf{Ah} - \kappa\mathbf{B}(\mathbf{x}_M - \mathbf{x}_S), \end{aligned} \tag{1}$$

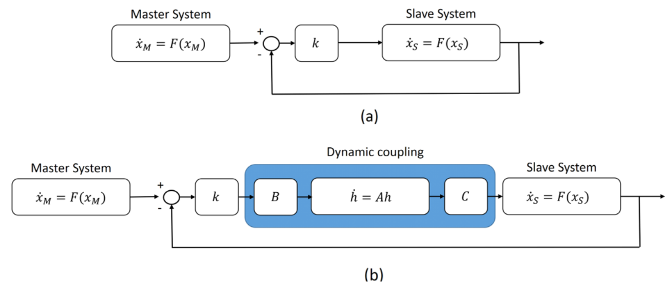

FIG. 1. Comparison between the master-slave coupling scheme (a) with a direct connection using only a coupling gain κ and (b) with the inclusion of a linear dynamical system to modulate the error feedback.

where $\mathbf{x_M} \in \mathbb{R}^n$ and $\mathbf{x_S} \in \mathbb{R}^n$ represent the vectors of the state variables for the master and slave systems, respectively, and $\mathbf{F}$ is the nonlinear function describing the dynamics of the hyperchaotic systems taken into consideration. The linear coupling system is modeled through the state variables $\mathbf{h} \in \mathbb{R}^2$, and $\mathbf{A}$ represents the state matrix here modeled as a mass-spring-damper system:

$$\mathbf{A} = \begin{bmatrix} -\alpha & 1 \\ -\gamma_1 & -\gamma_2 \end{bmatrix}, \tag{2}$$

where γ_1 and γ_2 are related to the undamped natural frequency and the damping ratio, whereas α is an additional term here introduced to increase the degrees of freedom while searching the suitable values of the parameters to synchronize the coupled systems. Furthermore, κ is the coupling strength, and $\mathbf{B} \in \mathbb{R}^{2\times n}$ and $\mathbf{C} \in \mathbb{R}^{n\times 2}$ represent the input and output matrices of the linear second-order coupling system. In detail, $\mathbf{B}$ indicates how to build the error driving signal from the state variables of master and salve to be processed by the dynamic coupling system, whereas the matrix $\mathbf{C}$ describes which variables of the slave system are subject to the control input.

The parameters of the coupling system have to be properly selected in order to obtain the master-slave synchronization. The selection can be performed either through extensive simulations trying to explore the different eligible combinations of the parameters or by analyzing the stability of the error dynamics, considered as a perturbed linear system.

A. Stability analysis

The parameters introduced in the coupling scheme have to be tuned to reach a synchronous behavior between the selected master and slave systems. In this section a series of conditions will be introduced. Looking to the linear dynamical coupling system, when the master and slave are synchronized (i.e., $\mathbf{x}_M = \mathbf{x}_S$), the coupling signal needs to exhaust its effect. To reach this behavior, A in Eq. (2) has to be a stable matrix with all the eigenvalues presenting a negative real part. If the parameters α, γ_1, and γ_2 are positive, this condition is verified.

To find further stability conditions without applying an analysis based on the master stability function, Eq. (1) can be decomposed into linear and nonlinear parts. The synchronization error dynamics for the master and slave systems can

TABLE I. Parameters used in the Chua system [Eq. (5)] to obtain a hyperchaotic behavior.

Parameter	Value
α_c	9.5
β_c	16
m_{c_0}	$-\frac{2}{7}$
m_{c_1}	$\frac{1}{7}$
k_{c_1}	-0.1
k_{c_2}	0.6
ω_c	0.03

be described by the following equation:

$$\dot{\mathbf{e}} = \mathbf{L_D}\mathbf{e} + \mathbf{p}(\mathbf{t}, \mathbf{e}), \tag{3}$$

where $\mathbf{e} := (\mathbf{x}_M - \mathbf{x}_S, \mathbf{h})^T$ and $\mathbf{p}(\mathbf{t}, \mathbf{e})$ is a perturbation due to the nonlinear terms that vanishes when the master and slave systems are synchronized.

On the basis of the application of stability theory to perturbed systems [25], to guarantee the local stability of the error system, $\mathbf{L_D} \in \mathbb{R}^{n+2\times n+2}$ has to be a stable matrix. It can be formalized as follow:

$$\mathbf{L_D} = \begin{bmatrix} \mathbf{L}_F & \mathbf{C} \\ -\kappa\mathbf{B} & \mathbf{A} \end{bmatrix}, \tag{4}$$

where $\mathbf{L}_F \in \mathbb{R}^{n\times n}$ is a constant matrix containing the coefficient of the linear part of the error dynamics between master and slave.

It can be noticed that the introduction of the dynamical coupling allows us to extend the classical static coupling where we can similarly define a matrix $\mathbf{L_S} \in \mathbb{R}^{n\times n}$ to be compared with $\mathbf{L_D}$. The available parameters present in $\mathbf{L_D}$ can be selected to extend the domain of κ where the synchronization is obtained.

III. SYNCHRONIZATION OF HYPERCHAOTIC SYSTEMS

To analyze the effect of the dynamic coupling in a master-slave configuration, compared with the static coupling, we selected two different hyperchaotic systems: the Chua and Saito circuits. In the following the two systems are analyzed and the presence of a synchronization regime, depending on the control parameters, is discussed.

A. Case study: Hyperchaotic Chua circuit

The previously depicted strategy has been applied to the hyperchaotic extension of the Chua circuit [26] that is characterized by the following equations:

$$\begin{aligned} \dot{x} &= \alpha_c[y - h^{\text{Chua}}(x)], \\ \dot{y} &= x - y + z + w, \\ \dot{z} &= -\beta_c y + w, \\ \dot{w} &= k_{c_1}x + k_{c_2}y + \omega_c w, \end{aligned} \tag{5}$$

where $h^{\text{Chua}}(x) = m_{c_1}x + 0.5(m_{c_0} - m_{c_1})(|x+1| - |x-1|)$. Choosing the parameters as reported in Table I, the system exhibits hyperchaotic behavior with two positive Lyapunov exponents.

We considered a static coupling mechanism and a dynamic one, as described in Eq. (1), applying the following input and output matrices:

$$\mathbf{B} = \begin{bmatrix} 0 & 0 & 0 & 0 \\ 0 & 0 & 1 & 0 \end{bmatrix}, \quad \mathbf{C} = \begin{bmatrix} 0 & 0 \\ 0 & 0 \\ 0 & 1 \\ 0 & 0 \end{bmatrix}. \tag{6}$$

The connection between the coupling system and the slave system is expressed through the matrix $\mathbf{C}$: the second variable of the linear coupling system is used as input for the third equation of the slave system. The input matrix $\mathbf{B}$ of the coupling system indicates that the error signal is evaluated comparing the third state variables of both master and slave systems and the error is used as input in the second dynamical equation of the linear coupling system. The selection of different input and output matrices can be easily performed in simulation obtaining different synchronization behaviors; however, in other cases more related to a physical implementation (e.g., electronic circuit), the access to all state variables may not be guaranteed.

The complete equations of the master and slave systems using either a static or a dynamic coupling are here reported:

Static coupling:

$$\begin{aligned} \dot{x}_M &= \alpha_c[y_M - h^{\text{Chua}}(x_M)], \\ \dot{y}_M &= x_M - y_M + z_M + w_M, \\ \dot{z}_M &= -\beta_c y_M + w_M, \\ \dot{w}_M &= k_{c_1}x_M + k_{c_2}y_M + \omega_c w_M, \\ \dot{x}_S &= \alpha_c[y_S - h^{\text{Chua}}(x_S)], \\ \dot{y}_S &= x_S - y_S + z_S + w_S, \\ \dot{z}_S &= -\beta_c y_S + w_S + \kappa(z_M - z_S), \\ \dot{w}_S &= k_{c_1}x_S + k_{c_2}y_S + \omega_c w_S. \end{aligned}$$

Dynamic coupling:

$$\begin{aligned} \dot{x}_M &= \alpha_c[y_M - h^{\text{Chua}}(x_M)], \\ \dot{y}_M &= x_M - y_M + z_M + w_M, \\ \dot{z}_M &= -\beta_c y_M + w_M, \\ \dot{w}_M &= k_{c_1}x_M + k_{c_2}y_M + \omega_c w_M, \\ \dot{x}_S &= \alpha_c[y_S - h^{\text{Chua}}(x_S)], \\ \dot{y}_S &= x_S - y_S + z_S + w_S, \\ \dot{z}_S &= -\beta_c y_S + w_S - h_2, \\ \dot{w}_S &= k_{c_1}x_S + k_{c_2}y_S + \omega_c w_S, \\ \dot{h}_1 &= -\alpha h_1 + h_2, \\ \dot{h}_2 &= -\gamma_1 h_1 - \gamma_2 h_2 - \kappa(z_M - z_S). \end{aligned} \tag{7}$$

We can start analyzing the static coupling: the characteristic piece-wise linear function h^{Chua} allows us to evaluate the matrix $L_S^{\text{Chua}} \in \mathbb{R}^{4\times 4}$ in the three different linear regions identified by the nonlinearity. In detail, we considered the following cases:

$$\begin{aligned} h^{\text{Chua}}(x) &= m_{c_1}x - (m_{c_0} - m_{c_1}) && \text{if} \quad x < -1, \\ h^{\text{Chua}}(x) &= m_{c_0}x && \text{if} \quad x < -1, \\ h^{\text{Chua}}(x) &= m_{c_1}x + (m_{c_0} - m_{c_1}) && \text{if} \quad x > 1. \end{aligned} \tag{8}$$

The first and third conditions produce the same L_S matrix, therefore we can consider:

$$\mathbf{L}_{S_i}^{\text{Chua}} = \begin{bmatrix} -h_i^{\text{Chua}}\alpha_c & \alpha_c & 0 & 0 \\ 1 & -1 & 1 & 1 \\ 0 & -\beta_c & -\kappa & 1 \\ k_{c_1} & k_{c_2} & 0 & w_c \end{bmatrix}, \tag{9}$$

where $i = \{a, b\}$, $h_a^{\text{Chua}} = m_{c_1}$, and $h_b^{\text{Chua}} = m_{c_0}$.

Analyzing the error dynamics for the master and slave with the static coupling, we can acquire information on the local stability. The characteristic polynomial of $\mathbf{L}_{S_a}^{\text{Chua}}$ is

$$P\left(\lambda_{L_{S_a}^{\text{Chua}}}\right) = \lambda^4 + (\kappa + 2.33)\lambda^3 + (2.33\kappa + 7.19)\lambda^2 + (21 - 8.81\kappa)\lambda + 0.38\kappa - 0.516. \tag{10}$$

To verify the asymptotic stability of the error system, we can apply the Routh-Hurwitz criteria obtaining the following constraints:

$$1.36 < \kappa < 2.37, \tag{11}$$

therefore when both the master and slave system state variables behave in the first region in Eq. (8), the synchronization manifold is locally asymptotically stable if the coupling strength is selected in a narrow region identified in Eq. (11). We can now investigate the effect of the dynamical coupling in this working region. The matrix $\mathbf{L_D} \in \mathbb{R}^{6\times 6}$ in Eq. (4) is here reported:

$$\mathbf{L}_{D_i}^{\text{Chua}} = \begin{bmatrix} -h_i^{\text{Chua}}\alpha_c & \alpha_c & 0 & 0 & 0 & 0 \\ 1 & -1 & 1 & 1 & 0 & 0 \\ 0 & -\beta_c & 0 & 1 & 0 & 1 \\ k_{c_1} & k_{c_2} & 0 & w_c & 0 & 0 \\ 0 & 0 & 0 & 0 & -\alpha & 1 \\ 0 & 0 & -\kappa & 0 & -\gamma_1 & -\gamma_2 \end{bmatrix}, \tag{12}$$

where $i = \{a, b\}$, $h_a^{\text{Chua}} = m_{c_1}$, and $h_b^{\text{Chua}} = m_{c_0}$. The presence of four state variables in the hyperchaotic system, increased to six with the introduction of the dynamic coupling, does not allow a complete parametric analysis of the matrix stability. To address the problem, a value must be assigned to the parameters of the coupling system, keeping κ as the only free parameter. Selecting for the coupling system the following parameters: $\alpha = 3$ and $\gamma_1 = \gamma_2 = \kappa/2$, the characteristic polynomial associated with $\mathbf{L}_{D_a}^{\text{Chua}}$ corresponding to the first linear region analyzed is

$$P\left(\lambda_{L_{D_a}^{\text{Chua}}}\right) = \lambda^6 + (0.5\kappa + 5.33)\lambda^5 + (4.16\kappa + 14.17)\lambda^4 + (13.57\kappa + 42.57)\lambda^3 + (23.05\kappa + 62.53)\lambda^2 + (15.71\kappa - 1.55)\lambda^1 + 0.11\kappa. \tag{13}$$

The range of κ that guarantees negative eigenvalues is

$$\kappa > 1.1, \tag{14}$$

which is wider with respect to the standard coupling.

Figure 2(a) shows the comparison between the two coupling mechanisms in terms of $\lambda_{\max}$ of the Jacobian matrix associated with the error system, as a function of the coupling strength. Extending the proposed analysis to the second region considering $i = b$, it can be verified that a range of κ that guarantees asymptotic stability for the error dynamics does not exist for either coupling strategy; this result is summarized in Fig. 2(b). The local analysis here performed does not allow us to reach a clear conclusion; therefore, we adopted the MSF as a global method to verify the presence of a synchronization manifold.

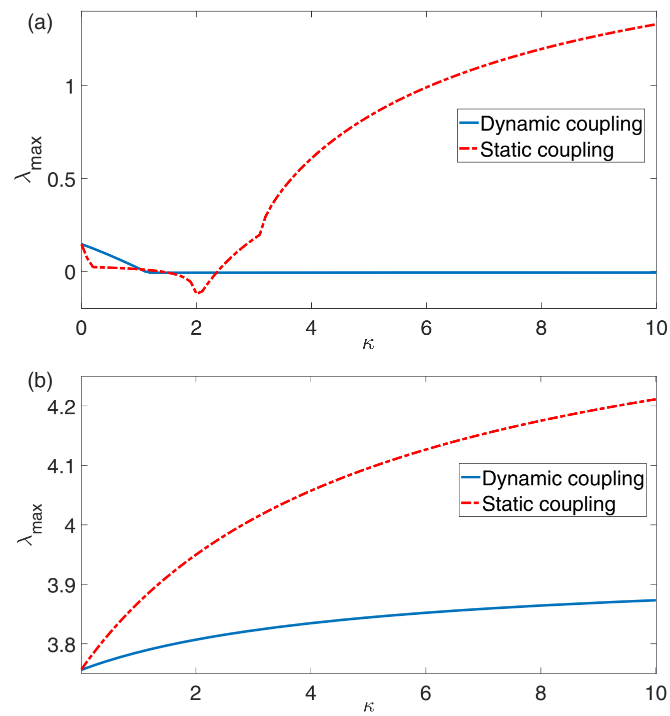

FIG. 2. Trend of the $\lambda_{\max}$ of the synchronization error dynamics as a function of the coupling strength for the static and dynamic coupling. The analysis for the (a) first and (b) second linear regions identified in the Chua circuit are both reported.

In Fig. 3 the largest Lyapunov exponent transverse to the synchronization manifold ($\Lambda_{\max}$), in relation to the coupling coefficient κ, is reported for both the static and dynamic coupling schemes. The global analysis demonstrates that the introduction of a dynamic coupling improves the range of κ that allows us to reach a synchronization regime. The trend

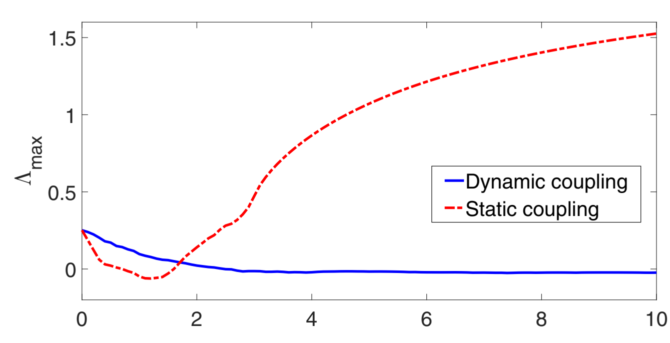

FIG. 3. Relation between the $\Lambda_{\max}$ and the coupling gain κ obtained applying the MSF in the case of static and dynamic coupling for the Chua circuit, with parameters $\alpha = 3$ and $\gamma_1 = \gamma_2 = \kappa/2$. The static coupling allows synchronization in the range $0.8 < \kappa < 1.6$ whereas the dynamic coupling extend the range to $\kappa > 2.5$.

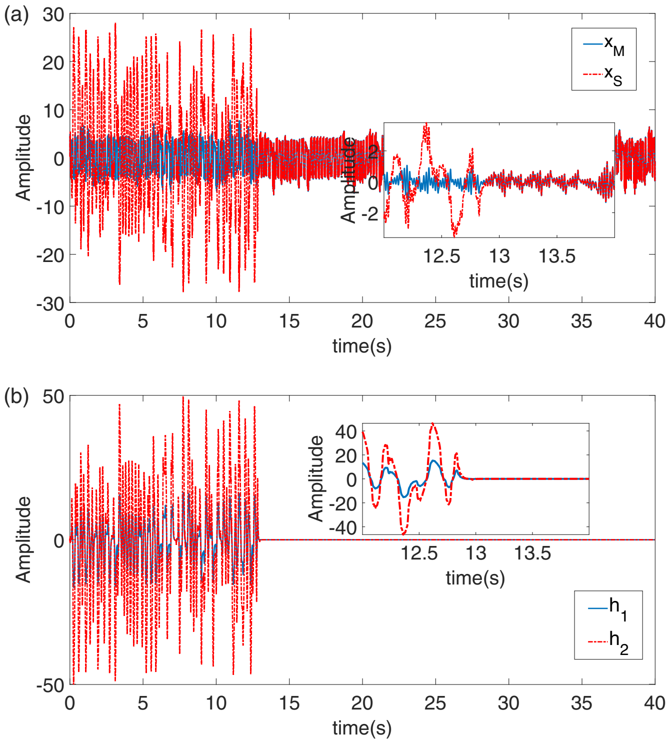

FIG. 4. Synchronization of two hyperchaotic Chua circuits. (a) Time evolution of the first state variable x for the master and slave system. (b) Trend of the state variable h_1 and h_2 of the second-order coupling system, when the coupling gain $\kappa = 3$ is selected.

of the first state variable for both master and slave systems (x_M, x_S) and the state variables of the coupling system (h_1, h_2), selecting $\kappa = 3$, are reported in Fig. 4: the master and slave systems, providing that the initial conditions behave in the basin of attraction of the hyperchaotic dynamics, after a short transitory, reach a complete synchronization, canceling the error signal. This is also demonstrated by the time evolution of the state variables of the coupling system that relax to zero in the absence of an input signal.

B. Case study: Saito circuit

The second case study reports the synchronization of two hyperchaotic Saito systems [5]. This system presents, as in the case of the Chua circuit, a single nonlinearity with a Piecewise linear shape. The dynamical equations of the master-slave with linear system coupling are here reported:

Static coupling:

$$\begin{aligned}
\dot{x}_M &= -z_M - w_M,\\
\dot{y}_M &= \gamma(2\delta y_M + z_M),\\
\dot{z}_M &= \rho(x_M - y_M),\\
\dot{w}_M &= \varepsilon^{-1}[x_M - h^{\mathrm{Saito}}(w_M)],\\
\dot{x}_S &= -z_S - w_S + \kappa(x_M - x_S),\\
\dot{y}_S &= \gamma(2\delta_S y_S + z_S),\\
\dot{z}_S &= \rho(x_S - y_S),\\
\dot{w}_S &= \varepsilon^{-1}[x_S - h^{\mathrm{Saito}}(w_S)].
\end{aligned}$$

Dynamic coupling:

$$\begin{aligned}
\dot{x}_M &= -z_M - w_M,\\
\dot{y}_M &= \gamma(2\delta y_M + z_M),\\
\dot{z}_M &= \rho(x_M - y_M),\\
\dot{w}_M &= \varepsilon^{-1}[x_M - h^{\mathrm{Saito}}(w_M)],\\
\dot{x}_S &= -z_S - w_S - h_2,\\
\dot{y}_S &= \gamma(2\delta_S y_S + z_S),\\
\dot{z}_S &= \rho(x_S - y_S),\\
\dot{w}_S &= \varepsilon^{-1}[x_S - h^{\mathrm{Saito}}(w_S)],\\
\dot{h}_1 &= -\alpha h_1 + h_2,\\
\dot{h}_2 &= -\gamma_1 h_1 - \gamma_2 h_2 - \kappa(x_M - x_S),
\end{aligned} \tag{15}$$

where $h^{\mathrm{Saito}}(w) = \begin{cases} w-(1+\eta) & \text{if} \quad w \geqslant \eta, \\ -\eta^{-1}w & \text{if} \quad |w| < \eta, \\ w+(1+\eta) & \text{if} \quad w \leqslant -\eta. \end{cases}$

Choosing the system parameters as reported in Table II, each Saito system exhibits hyperchaotic behavior with two positive Lyapunov exponents. For this system we selected the first state variable for the generation of the error feedback between master and slave. Following the same procedure reported in Sec. III A we can identify, for the static coupling scheme, two different $\mathbf{L}_S$ matrices:

$$\mathbf{L}_{S_i}^{\mathrm{Saito}} = \begin{bmatrix} -k & 0 & -1 & -1 \\ 0 & 2\gamma\delta & 1 & 0 \\ \rho & -\rho & 0 & 0 \\ \varepsilon^{-1} & 0 & 0 & -h_i^{\mathrm{Saito}}\varepsilon^{-1} \end{bmatrix}, \tag{16}$$

where $i = \{a, b\}$, $h_a^{\mathrm{Saito}} = 1$ when $w \leqslant -1 \cup w \geqslant 1$, and $h_b^{\mathrm{Saito}} = -\eta^{-1}$ when $-1 < w < 1$.

The characteristic polynomial of $\mathbf{L}_{S_a}^{\mathrm{Saito}}$ and $\mathbf{L}_{S_b}^{\mathrm{Saito}}$ can be analyzed to verify the interval of acceptable coupling gain that produces a Hurwitz matrix:

$$\begin{aligned}
1.88 &< \kappa < 7.45 \text{ for } L_{S_a}^{\mathrm{Saito}},\\
1.90 &< \kappa < 2.88 \text{ for } L_{S_b}^{\mathrm{Saito}}.
\end{aligned} \tag{17}$$

Therefore, there is a regime of κ, obtained from the intersection between the acceptable values for the two working regions, in which the synchronization manifold is locally stable.

The dynamical coupling system was also considered using the following parameters: $\alpha = 100$ and $\gamma_1 = \gamma_2 = \kappa/2$. The

TABLE II. Parameters used in the Saito system [Eq. (15)] to obtain a hyperchaotic behavior.

Parameter	Value
γ	1
ρ	14
ε^{-1}	0.01
η	1
δ	0.94

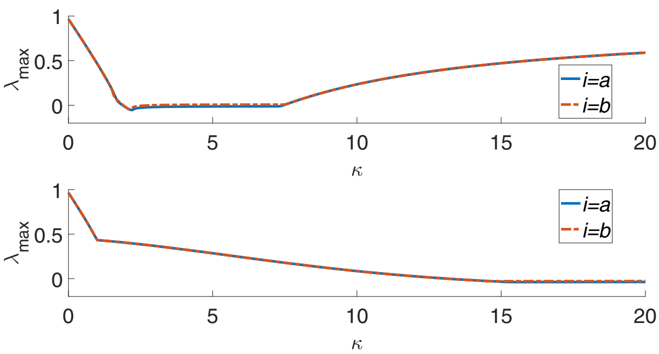

FIG. 5. Trend of the $\lambda_{\max}(\kappa)$ for the synchronization error dynamics of the linear restriction of the hyperchaotic Saito circuit in the presence of either static (top panel) or dynamic (bottom panel) coupling.

$\mathbf{L}_D$ matrices are described in the following:

$$\mathbf{L}_{D_i}^{\text{Saito}} = \begin{bmatrix} 0 & 0 & -1 & -1 & 0 & 1 \\ 0 & 2\gamma\delta & 1 & 0 & 0 & 0 \\ \rho & -\rho & 0 & 0 & 0 & 0 \\ \varepsilon^{-1} & 0 & 0 & -h_i^{\text{Saito}}\varepsilon^{-1} & 0 & 0 \\ 0 & 0 & 0 & 0 & -\alpha & 1 \\ -\kappa & 0 & 0 & 0 & -\gamma_1 & -\gamma_2 \end{bmatrix}. \tag{18}$$

In this case for both regions ($i = a$ and $i = b$), the range that guarantees the local stability is $\kappa > 13.13$. The evaluation of $\lambda_{\max}$ for the matrices $\mathbf{L}_S^{\text{Saito}}$ and $\mathbf{L}_D^{\text{Saito}}$ as function of κ is shown in Fig. 5; when $\lambda_{\max} < 0$ we have local stability for the synchronization manifold. Independent of the linear region considered, with a static coupling a narrow region of allowable κ is identified, whereas the dynamic coupling enlarges the range of κ eliminating the upper boundary. The nonlinear analysis performed with the MSF confirms these results as demonstrated in Fig. 6. In detail the range of κ obtained from the linear analysis is conservative if compared with the global stability results obtained from the MSF technique.

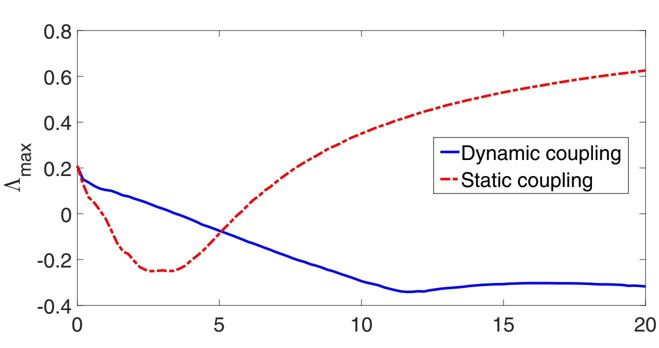

FIG. 6. Relation between the $\Lambda_{\max}$ and the coupling gain κ obtained applying the MSF for the static and dynamic coupling for the Saito systems, with parameters $\alpha = 100$ and $\gamma_1 = \gamma_2 = \kappa/2$. The static coupling allows synchronization in the range $0.9 < \kappa < 5.6$, whereas the dynamic coupling extends the range to $\kappa > 3.6$.

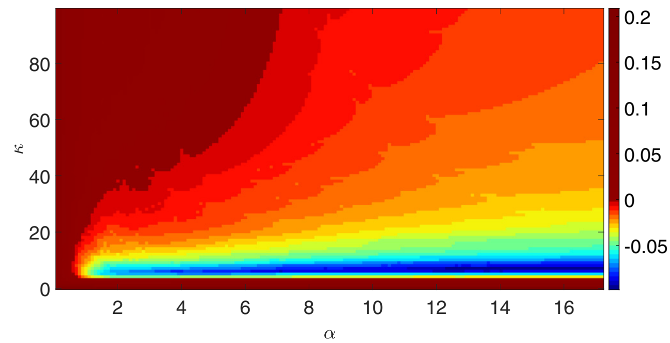

FIG. 7. Map of the maximum Lyapunov exponent transverse to the synchronization manifold, as function of α and κ, for the Saito circuit with dynamic coupling. The other parameters of the second-order linear coupling system are $\gamma_1 = \gamma_2 = \kappa$.

The parameters adopted for the dynamical coupling can modify the results obtained as demonstrated in Fig. 7 where the MSF for the Saito circuit with dynamic coupling is reported for a different value of the parameters $\gamma_1 = \gamma_2 = \kappa$ and as functions of κ and α. When α is too small, the synchronization cannot be achieved independently of the value chosen for κ. Moreover, to enlarge the range of κ that guarantees a stable synchronization we need to increase α. In the following section we will analyze these aspects providing a series of qualitative and quantitative indications on the selection of the suitable coupling system parameters under certain conditions.

IV. PARAMETER SELECTION

To better understand the effect of the dynamical coupling and the role of the parameters α, γ_1, and γ_2 used in the model and arbitrarily set in the case studies previously presented, we are now analyzing in detail the coupling system. The transfer function of the coupling system, including the coupling strength κ, considering that the external input acts on the second state variable (h_2) and that the output is generated by the same state variable, is the following:

$$G(s) = \kappa \frac{s + \alpha}{s^2 + (\alpha + \gamma_2)s + \alpha\gamma_2 + \gamma_1}. \tag{19}$$

The system presents a zero in $s = \alpha$ and two poles. Supposing we select $\alpha = 100$ and $\gamma_1 = \gamma_2 = \kappa/2$ as in the previous analysis with the Saito circuit, the position of the poles as a function of κ is reported in Fig. 8.

From this analysis we can underline two important considerations:

(i) The system is almost overdamped; in fact, the damping ratio $\xi = \frac{\alpha+\gamma_2}{2\sqrt{\gamma_1+\alpha\gamma_2}}$ with the selected parameters presents a minimum value of $\xi_{\min} = 0.995$.

(ii) The effect of the zero in $G(s)$ is almost completely compensated for by one of the poles that is next to it. For low values of κ (i.e., $\kappa < 250$) λ_1 and then λ_2 are next to the zero position, as reported in Fig. 8.

By using the Bode diagram as shown in Fig. 9, we can verify that there is a band of frequencies that is modulated by κ, in which the behavior of the system can be approximated to a fixed gain whose value can be calculated from Eq. (19):

$$G(0) = \kappa \frac{\alpha}{\alpha\gamma_2 + \gamma_1}. \tag{20}$$

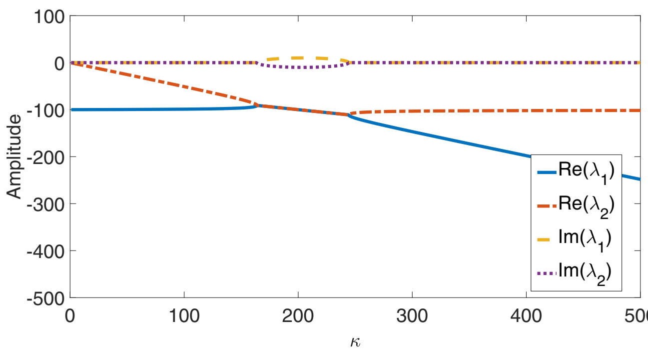

FIG. 8. Change of the poles for the transfer function in Eq. (19) depending on the coupling strength κ. The other parameters are $\alpha = 100$ and $\gamma_1 = \gamma_2 = \kappa/2$.

Imposing the parameters adopted in the hyperchaotic Saito circuit study, we obtain $G(0) = 2\frac{100}{100+1} = 1.98$, which is independent from the parameter κ. From the analysis performed in Sec. III B with the MSF, the static coupling guarantees synchronization in the range $0.9 < \kappa < 5.6$; and $G(0)$, obtained by adopting the dynamic coupling system, is included in this range.

Therefore, we can state that if $\exists\ \kappa_c \in [a_k, b_k]$, which allows us to synchronize two systems coupled in a master-slave configuration with a static gain, it is possible to create a dynamic coupling system that extends the range of allowable coupling strength, eliminating the upper bound. To obtain this effect it is possible to select $\gamma_1 = \gamma_2 = \kappa/\kappa_c$ and α large enough to guarantee a good zero-pole compensation in $G(s)$. In this case the dynamical coupling system leads to a stable synchronization for $\kappa > \kappa_{\min}$ that guarantees, in the band of frequencies of interest, an admissible attenuation of the modules and phase delay introduced by the dynamical coupling. As the coupling gain increases, the behavior of the dynamic coupling system will be more and more similar to a static gain for which synchronization is already guaranteed.

Alternatively it is possible to select κ_c and α so as to verify the following conditions:

$$\kappa_c \frac{\alpha}{\alpha + 1} \in [a_k, b_k]. \tag{21}$$

In this case the problem is that for low α values the zero-pole compensation is less precise and the system gain is no longer constant as the frequencies change, so the κ region that guarantees synchronization could be absent or with an upper-bound limitation as previously shown in Fig. 7.

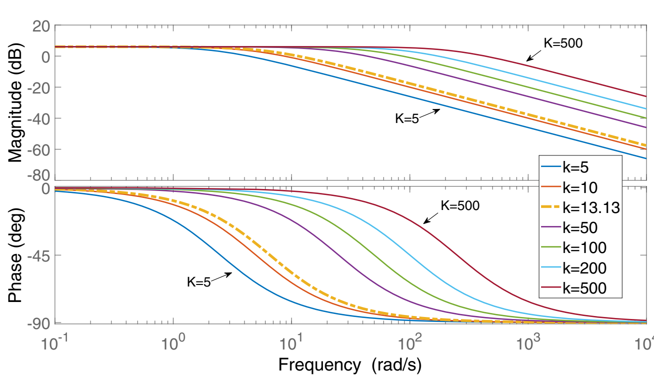

FIG. 9. Bode diagram for the coupling system in Eq. (19) with parameters $\alpha = 100$, $\gamma_1 = \gamma_2 = k/2$, for different values of κ.

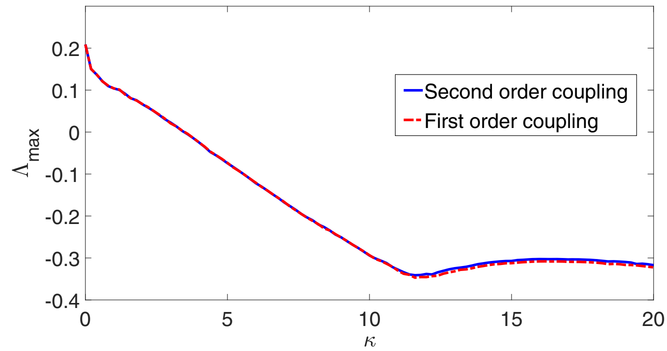

FIG. 10. Relation between $\Lambda_{\max}$ and the coupling gain κ obtained applying the MSF for the first- and second-order dynamic coupling in the Saito systems, with parameters: $\alpha = 100$, $\gamma_1 = \gamma_2 = \kappa/2$ for the second-order coupling and $\gamma = \kappa/2$ for the first-order coupling.

Considering the Saito circuit, if we select $\kappa_c = 1$, we can easily verify that selecting $a_k = 0.9$, as obtained from the MSF with the static coupling (as shown in Fig. 6), to satisfy the constraint introduced in Eq. (21) we need to impose $\alpha > 9$. The results reported in Fig. 7 show that the constraint obtained on α represents the transition from a limited region to an unlimited one in terms of values of κ that guarantee synchronization with the dynamic coupling. By changing the parameters we can find new ranges of synchronization and Eq. (21) gives a useful indication that can be applied when α is sufficiently large, as in the previously reported cases.

From this analysis it is possible to deduce that using the strategy of selecting α sufficiently large, given that the dynamic coupling system presents a zero-pole simplification, it is possible to reduce the order of the coupling system. This possibility, as analyzed in [23], leads to a possible reduction of the admissible κ range if the unique parameter γ of the first-order dynamic coupling system is set to a constant value. But, as demonstrated above, setting $\gamma = \kappa/\kappa_c$ all the considerations previously discussed are verified and the master-slave systems will synchronize in the same interval of κ as shown in Fig. 10.

V. APPLICATIONS IN WEIGHTED NETWORKS

The application of a dynamical coupling between hyperchaotic systems introduces important advantages if compared with a static one with a limited effort in terms of cost and complexity, due to the introduction of two linear dynamic equations to the master-slave system. This approach can be further appreciated when it becomes an instrument useful

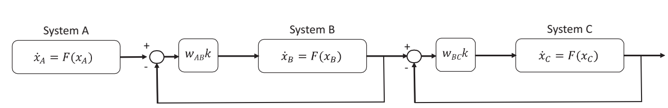

FIG. 11. Chain of three systems connected using a static gain κ weighted by parameters w that are associated to the each link.

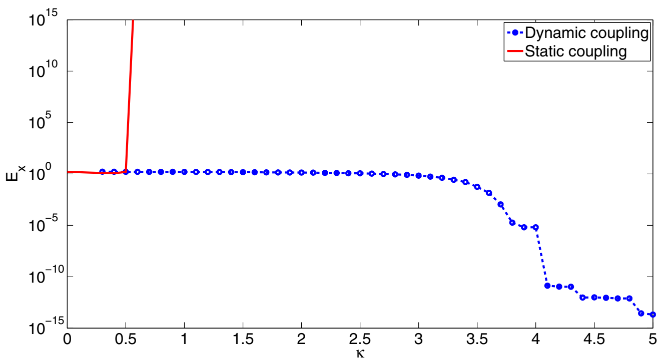

FIG. 12. Trend of the synchronization error evaluated in a directed chain of three hyperchaotic Saito systems with static and dynamic coupling. The parameters adopted for the dynamic coupling are $\alpha_{AB} = \alpha_{BC} = 100$ and $\gamma_{1AB} = \gamma_{2AB} = 5\kappa$ $\gamma_{1BC} = \gamma_{2BC} = \kappa/2$. The synchronization error E_x is evaluated on the last 20 s of a simulation of 1000 s mediated over 10 trials for each case.

in systems that cannot be synchronized adopting a static coupling mechanism. An interesting case study is to consider extending the master-slave mechanism to a simple directed weighted network. Therefore, we can consider a simple case in which three identical hyperchaotic systems are connected, creating an open chain as reported in Fig. 11 where the static connection is considered. Besides the static coupling gain, the network is characterized by a weighted graph in which each connection contains a different additional weight (i.e., w_{AB} and w_{BC}).

The Laplacian matrix of the network directed weighted network can be easily evaluated:

$$\mathbf{L} = \kappa \begin{bmatrix} 0 & 0 & 0 \\ -w_{AB} & w_{AB} & 0 \\ 0 & -w_{BC} & w_{BC} \end{bmatrix}. \tag{22}$$

To guarantee synchronization in the developed network, it is necessary that the eigenvalues of the Laplacian matrix different from the null ones have to be confined to the stable region associated with the κ gain as evaluated with the MSF [20].

Considering for each node the equation of the hyperchaotic Saito circuit, and choosing as link weights the values $w_{AB} = 1$ and $w_{BC} = 10$, it can be verified that the eigenvalues of $\mathbf{L}$ are $\lambda_1 = 10\kappa$ and $\lambda_2 = \kappa$ that needs to behave in the region $]0.9,5.6[$ as evaluated with the MSF with the static coupling case and previously reported in Fig. 6. It can be easily verified that this condition cannot be satisfied because there is no value of κ that guarantees both Laplacian eigenvalues inside the synchronization range. On the contrary, applying the dynamic coupling, the synchronization range is extended to $]3.6, +\infty[$ and both Laplacian eigenvalues can behave in this region choosing $\kappa > 3.6$.

These results have been verified through extensive simulations, as reported in Fig. 12, analyzing the synchronization error (E_x) of the network for different values of κ with both static and dynamic coupling. E_x is evaluated as the mean-square error among the first state variable of the first chain node, used as reference, and the other two nodes, mediated on a time window and on multiple simulations with different initial conditions. The obtained results demonstrate that the static coupling is not able to solve the problem whereas the dynamic coupling guarantees a solution for a wide range of coupling gain.

This approach can be further extended to more complex networks where the dynamic coupling mechanism becomes a relevant tool for dealing with the synchronization problem.

VI. CONCLUSIONS

The problem of synchronization can be addressed using different techniques depending on the connection scheme and control mechanisms. Hyperchaotic systems introduce further complexity to the synchronization problem, which can be solved by increasing the number of coupled variables used to control the slave system. In this work we presented a comparison in terms of synchronization domain, between identical hyperchaotic systems coupled in a master-slave configuration through either a static gain or a linear dynamical system. The advantages of the dynamic coupling, already highlighted for chaotic systems, are here verified in the presence of systems with multiple positive Lyapunov exponents. The assessment of the approach was concentrated on two specific systems: the hyperchaotic Chua and Saito circuits. The analysis of synchronization was carried out using a linear simplification based on the perturbation analysis for acquiring local information and a global method based on the MSF to compare the results.

The application to hyperchaotic systems, due to the increase in the number of equations with respect to chaotic systems, leads to a more complex symbolic analysis for the verification of the local stability of the synchronization manifold and, therefore, it is important to set the value of some parameters of the coupling system before being able to proceed to an analytical calculation of the synchronization performances. This aspect has been addressed by proposing a strategy to extend the allowable range of the coupling strength, obtained with the static coupling, eliminating the presence of an upper bound adopting a second-order linear coupling system that, under specific conditions, can be reduced to a first-order one. Finally, the importance of the dynamic coupling mechanism was demonstrated with an application to weighted networks. We reported a paradigmatic case showing how the synchronization of weighted networks takes advantage of the open region of admissible coupling gains introduced with dynamic coupling, solving a synchronization problem in a case where the standard coupling scheme is not able to find a suitable solution.

[1] S. Boccaletti, J. Kurths, G. Osipov, D. L. Valladares, and C. S. Zhou, The synchronization of chaotic systems, Phys. Rep. **366**, 1 (2002).

[2] M. Frasca, L. V. Gambuzza, A. Buscarino, and L. Fortuna, *Synchronization in Networks of Nonlinear Circuits: Essential Topics with Matlab code* (Springer, Berlin, 2018).

[3] W. Kinzel, A. Englert, and I. Kanter, On chaos synchronization and secure communication, Philos. Trans. R. Soc. A: Math. Phys. Eng. Sci. **368**, 379 (2010).

[4] E. Arena, P. Arena, and L. Patanè, Efficient hexapodal locomotion control based on flow-invariant subspaces, in *18th World Congress of the International Federation of Automatic Control (IFAC), 2011*, edited by S. Bittanti (Elsevier Science Direct, 2011), p. 13758.

[5] A. Buscarino, L. Fortuna, and M. Frasca, *Essentials of Nonlinear Circuit Dynamics with MATLAB and Laboratory Experiments* (CRC, Boca Raton, FL, 2017).

[6] A. Buscarino, L. Fortuna, M. Frasca, and G. Sciuto, *A Concise Guide to Chaotic Electronic Circuits* (Springer International, Heidelberg, 2014).

[7] G. Katriel, Synchronization of oscillators coupled through an environment, Physica D **237**, 2933 (2008).

[8] P. F. Curran, J. A. K. Suykens, and L. O. Chua, Absolute stability theory and master-slave synchronization, Int. J. Bifurcation Chaos **7**, 2891 (1997).

[9] Z. H. Guan, D. J. Hill, and J. Yao, A hybrid impulsive and switching control strategy for synchronization of nonlinear systems and application to Chua's chaotic circuit, Int. J. Bifurcation Chaos **16**, 229 (2006).

[10] L. Huang, Q. Chen, Y. C. Lai, and L. M. Pecora, Generic behavior of master-stability functions in coupled nonlinear dynamical systems, Phys. Rev. E **80**, 036204 (2009).

[11] R. Brown, N. F. Rulkov, and E. R. Tracy, Modeling and synchronizing chaotic systems from time-series data, Phys. Rev. E **49**, 3784 (1994).

[12] A. Buscarino, L. Fortuna, M. Frasca, and G. Sciuto, Chua's circuits synchronization with diffusive coupling: New results, Int. J. Bifurcation Chaos **19**, 3103 (2009).

[13] L. M. Pecora and T. L. Carroll, Synchronization in Chaotic Systems, Phys. Rev. Lett. **64**, 821 (1990).

[14] D. M. Abrams and S. H. Strogatz, Chimera States for Coupled Oscillators, Phys. Rev. Lett. **93**, 174102 (2004).

[15] D. M. Abrams, R. Mirollo, S. H. Strogatz, and D. A. Wiley, Solvable Model for Chimera States of Coupled Oscillators, Phys. Rev. Lett. **101**, 084103 (2008).

[16] A. Bergner, M. Frasca, G. Sciuto, A. Buscarino, E. J. Ngamga, L. Fortuna, and J. Kurths, Remote synchronization in star networks, Phys. Rev. E **85**, 026208 (2012).

[17] A. Buscarino, M. Frasca, L. V. Gambuzza, and P. Hövel, Chimera states in time-varying complex networks, Phys. Rev. E **91**, 022817 (2015).

[18] L. V. Gambuzza and M. Frasca, Pinning control of chimera states, Phys. Rev. E **94**, 022306 (2016).

[19] P. Hövel, A. Viol, P. Loske, L. Merfort, and V. Vuksanović, Synchronization in functional networks of the human brain, J. Nonlinear Sci. **1**, 1 (2018).

[20] L. M. Pecora and T. L. Carroll, Master Stability Functions for synchronized Coupled Systems, Phys. Rev. Lett. **80**, 2109 (1998).

[21] K. Pyragas, Predictable chaos in slightly perturbed unpredictable chaotic systems, Phys. Lett. A **181**, 203 (1993).

[22] A. Buscarino, L. Fortuna, and M. Frasca, Experimental robust synchronization of hyperchaotic circuits, Physica D **238**, 1917 (2009).

[23] J. Pena Ramirez, A. Arellano-Delgado, and H. Nijmeijer, Enhancing master-slave synchronization: The effect of using a dynamic coupling, Phys. Rev. E **98**, 012208 (2018).

[24] A. Lassoued and O. Boubaker, On new chaotic and hyperchaotic systems: A literature survey, Nonlinear Anal. **21**, 770 (2016).

[25] L. Khalil, *Nonlinear Systems*, 3rd ed. (Prentice-Hall, New York, 2002).

[26] L. Fortuna, M. Frasca, and M. Xibilia, *Chua's Circuit Implementations: Yesterday, Today and Tomorrow*, World Scientific Series on Nonlinear Science: Series A (World Scientific, Singapore, 2009).